

Orion fluctuations: New material 2015-10

W. J. Henney, C. R. O'Dell, G. J. Ferland, M. Peimbert

1. Temperature and density diagnostics from the MUSE data

1.1. Maps at constant signal-to-noise

1.2. Diagnostic plots

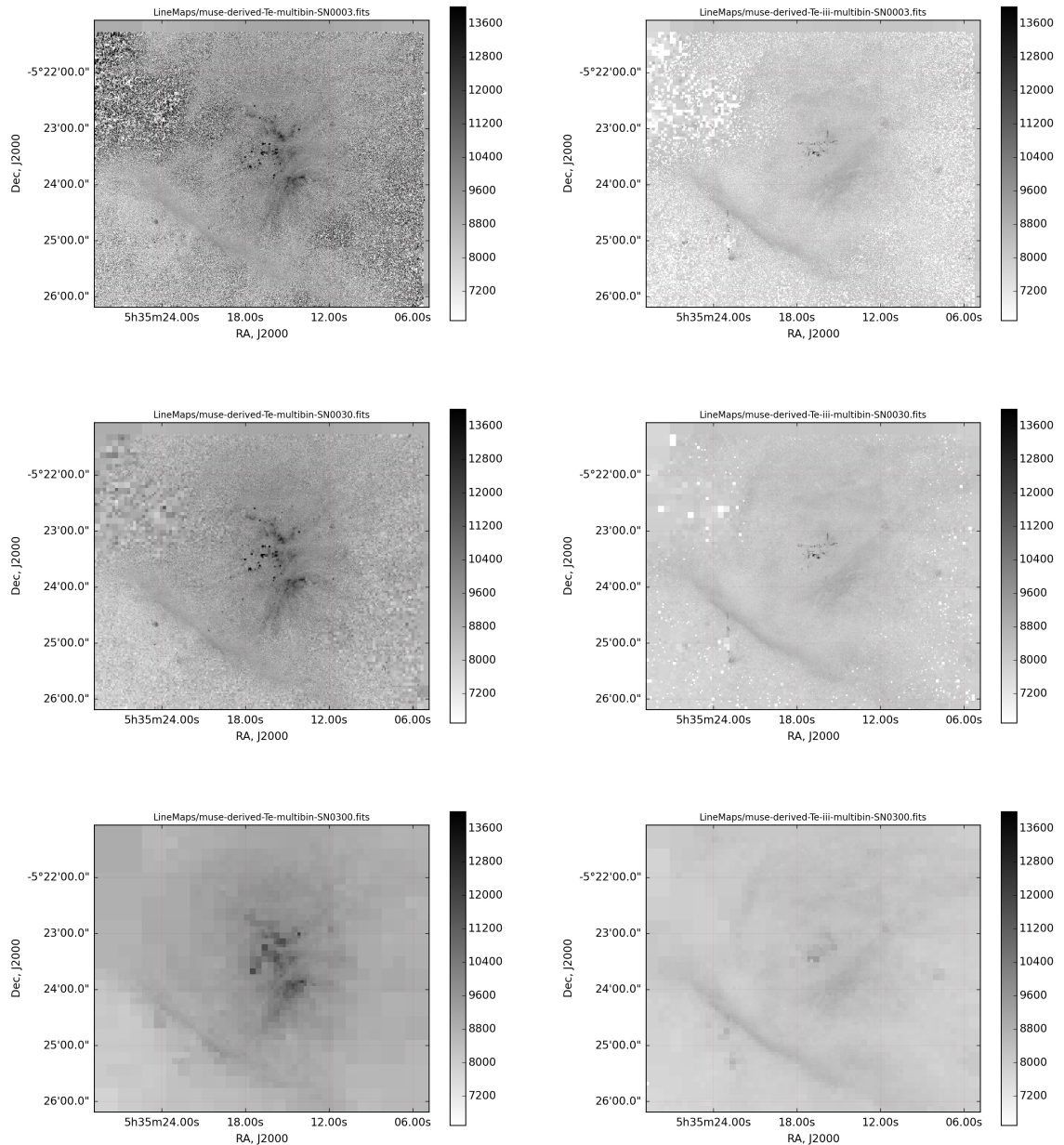


Fig. 1.— Temperature maps from MUSE spectra, adaptively binned to give constant signal-to-noise ratios of, top to bottom, 3, 30, and 300. Left column [N II] temperature, right column [S III] temperature.

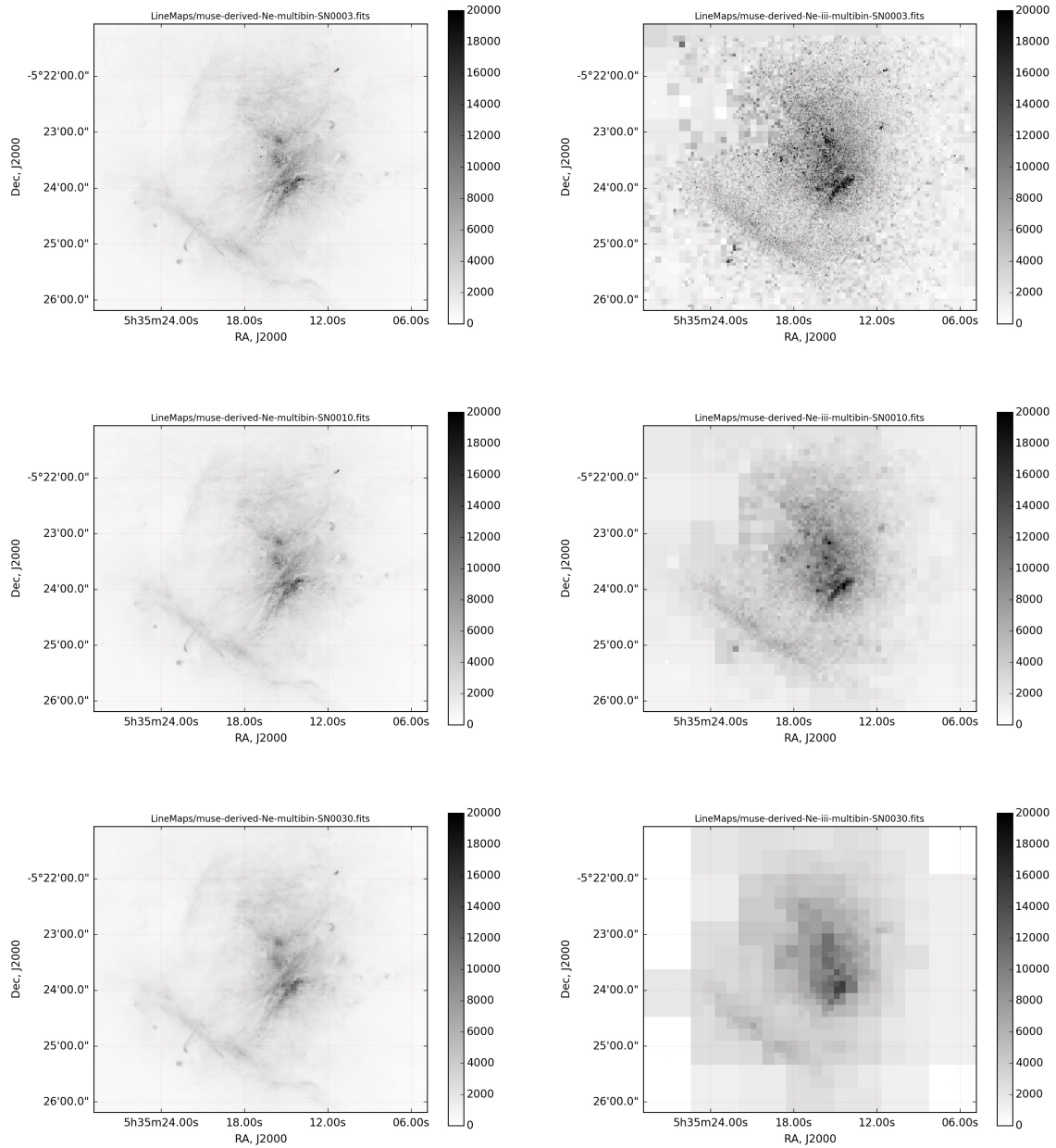


Fig. 2.— Density maps at different signal-to-noise ratio.

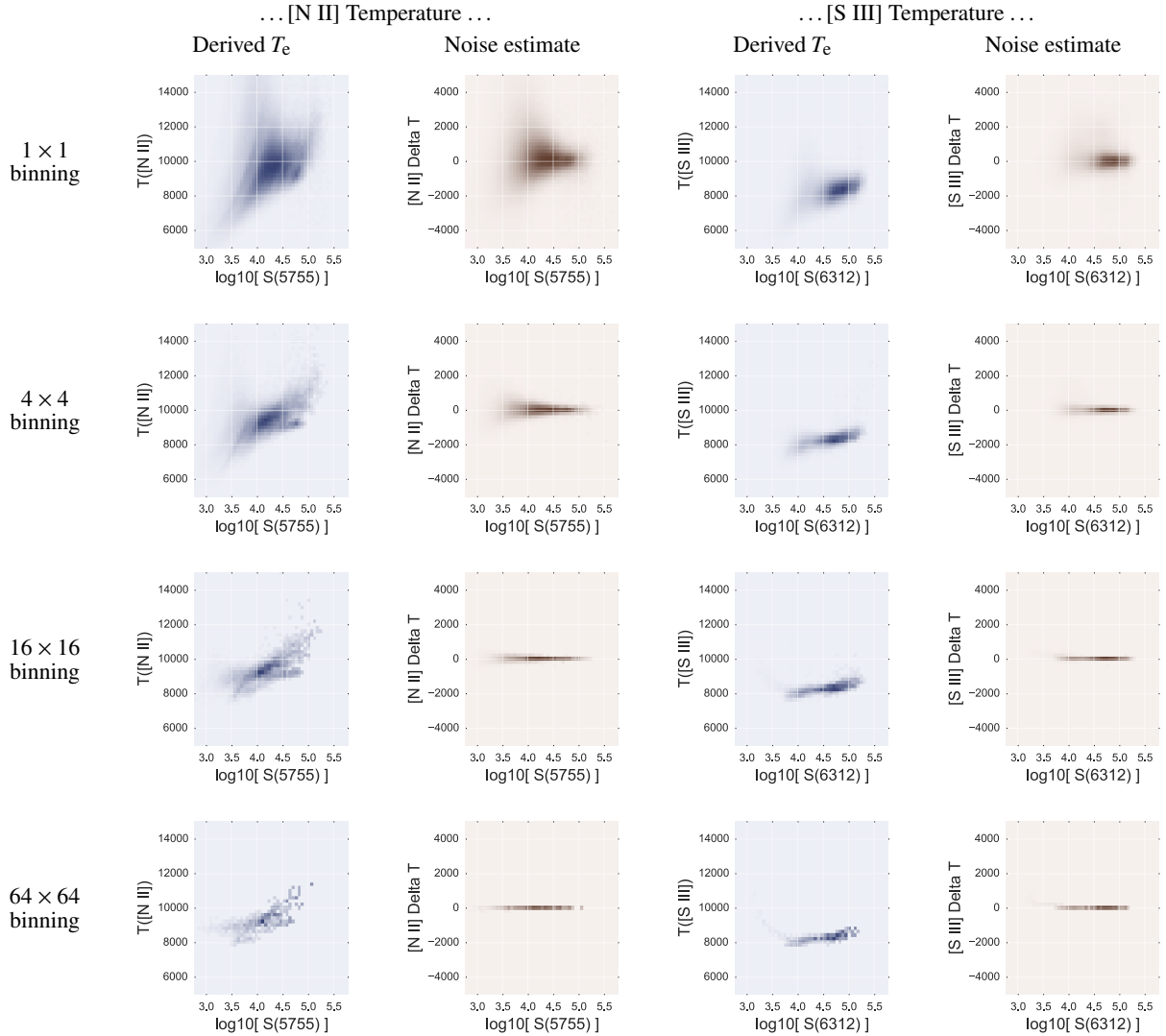


Fig. 3.— Derived temperature versus surface brightness as a function of binning for the full MUSE field

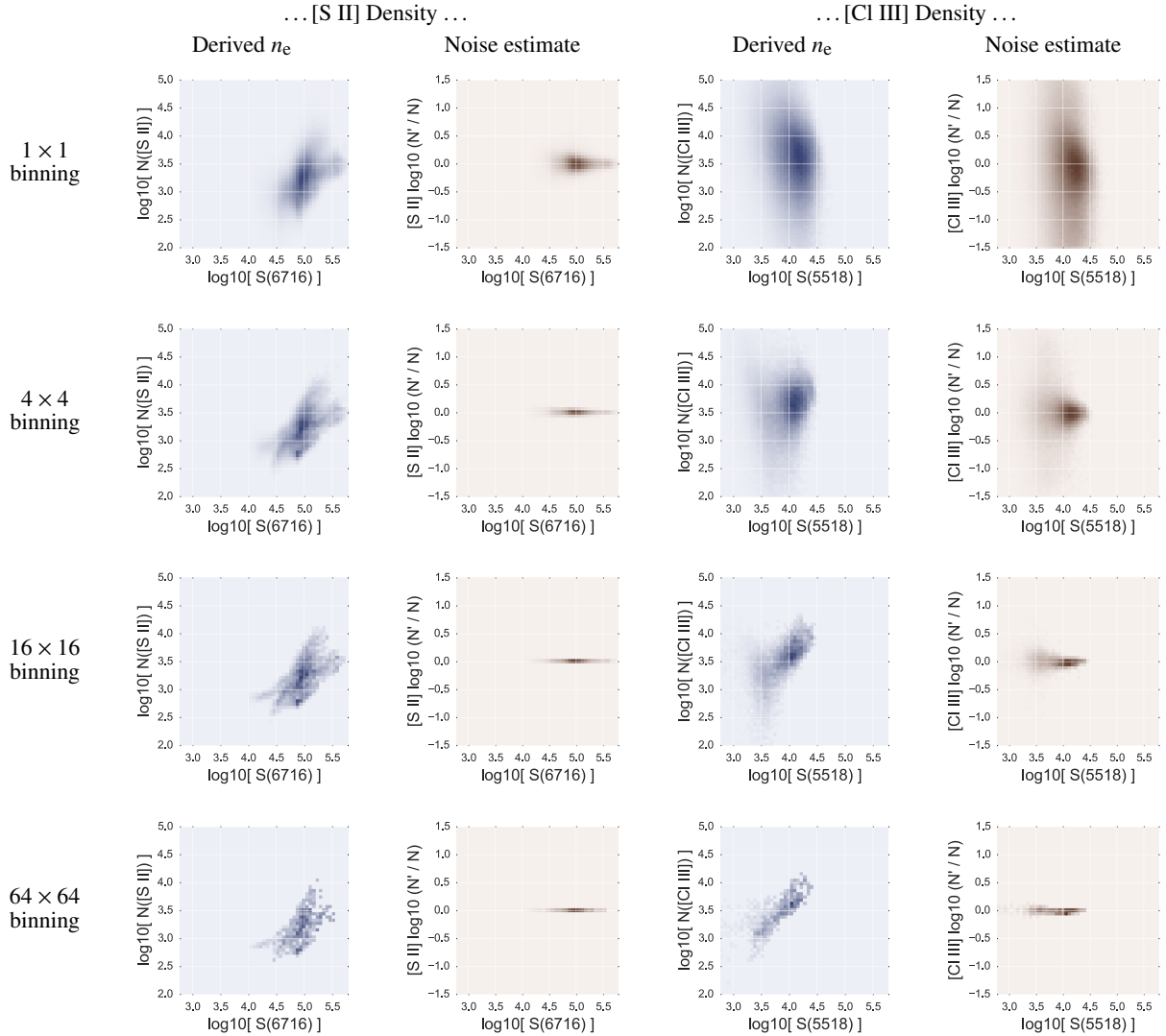


Fig. 4.— Derived density versus surface brightness as a function of binning for the full MUSE field

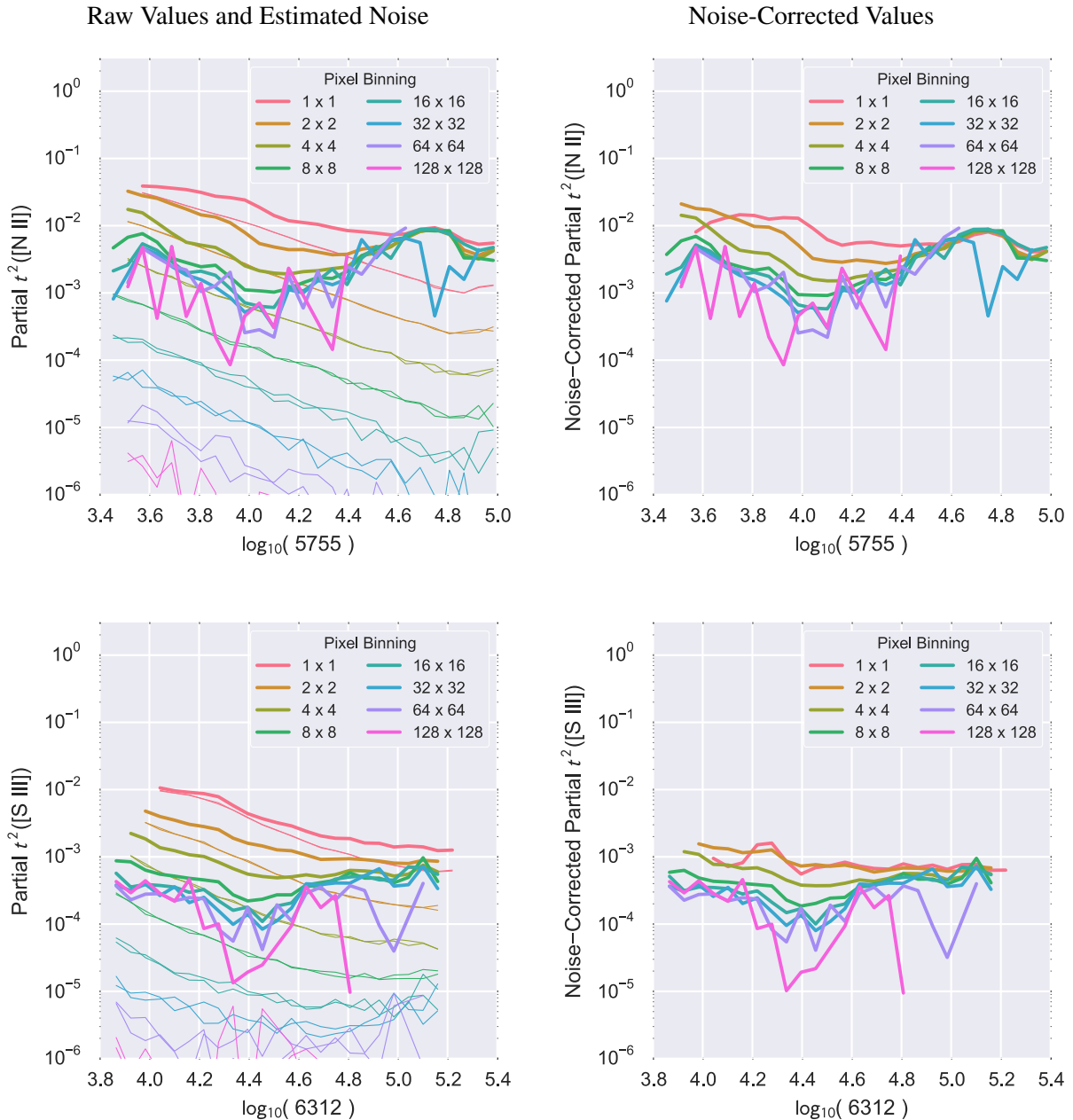


Fig. 5.— Partial t^2 versus brightness for different pixel binnings. In all cases t^2 is calculated from a robust version of the variance: $t^2 = \hat{\sigma}^2(T)/\text{median}(T)^2$ $\hat{\sigma} = 0.7413\text{IQR}$

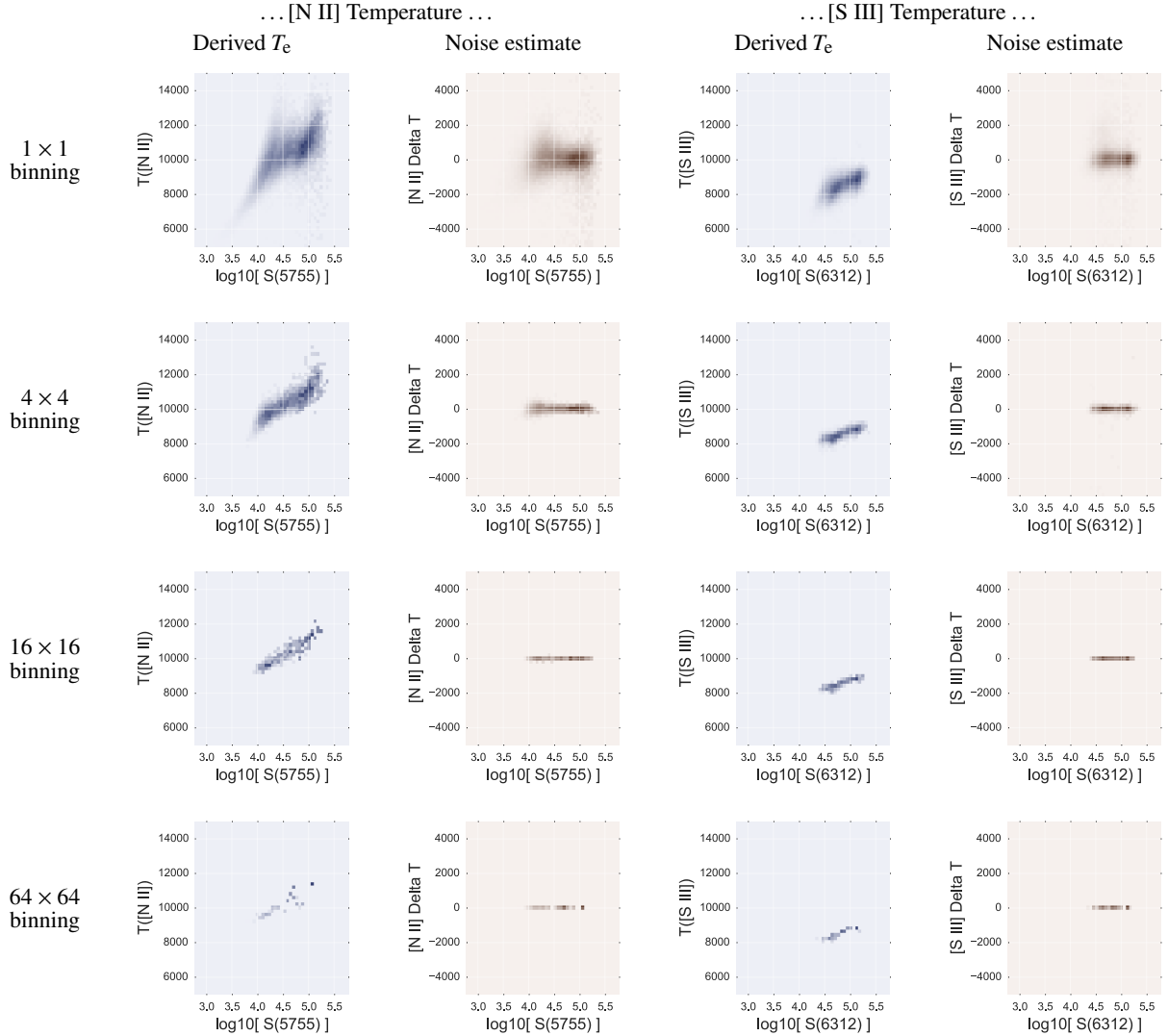


Fig. 6.— Derived temperature versus surface brightness as a function of binning for the MUSE data restricted to the WFC3 field.

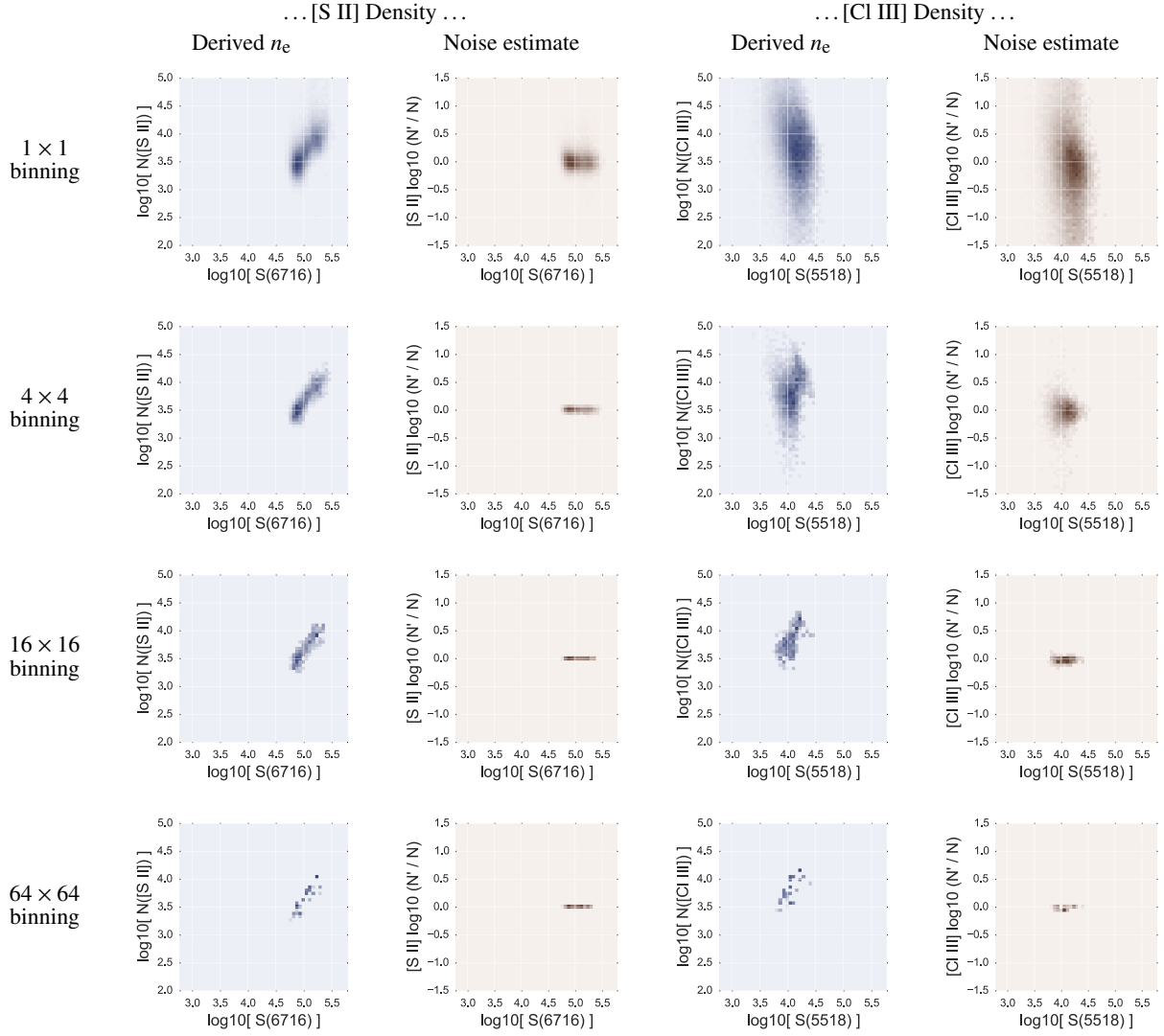


Fig. 7.— Derived density versus surface brightness as a function of binning for the MUSE data restricted to the WFC3 field.

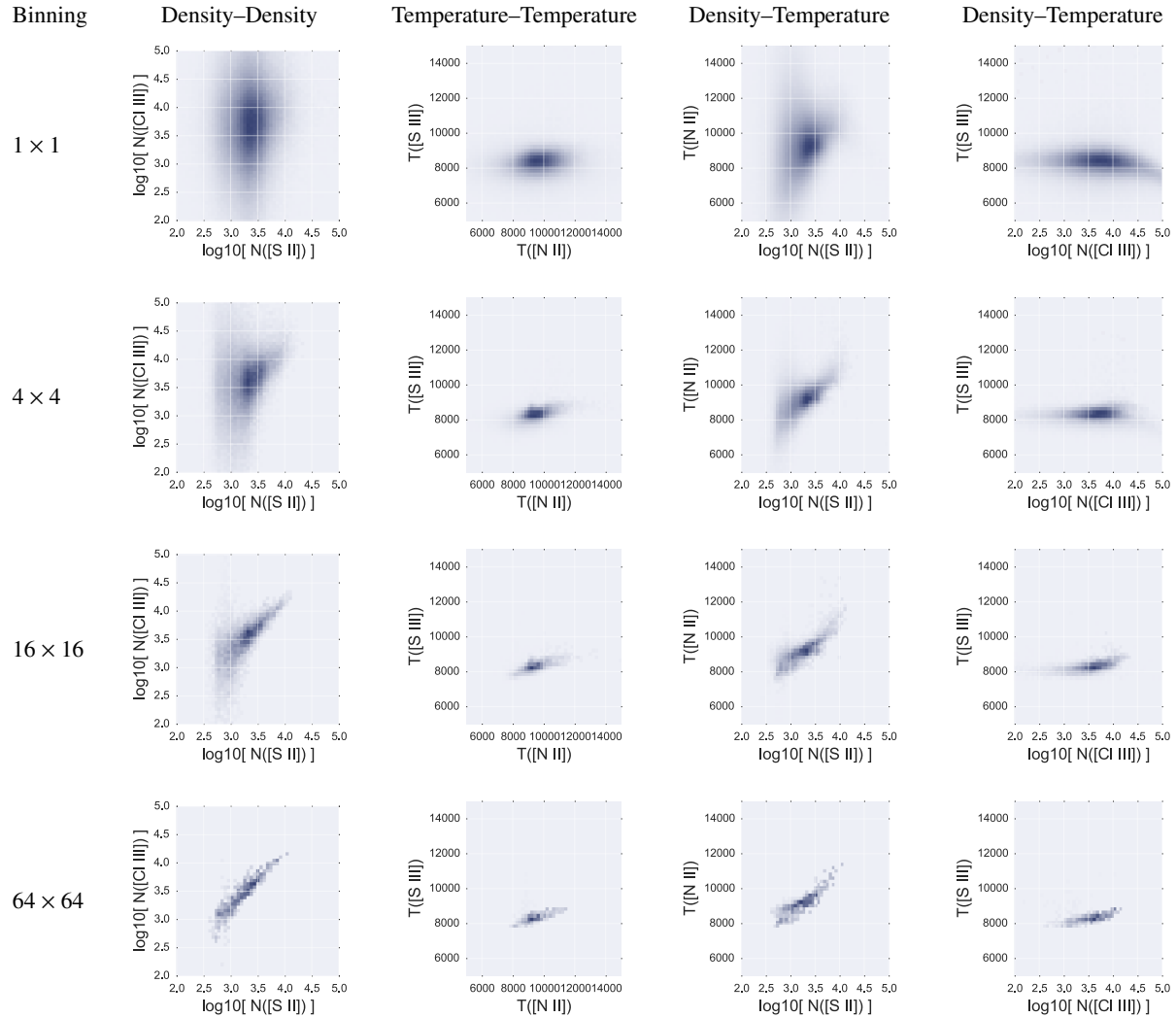


Fig. 8.— Correlations between derived densities and temperatures as a function of binning for the full MUSE field

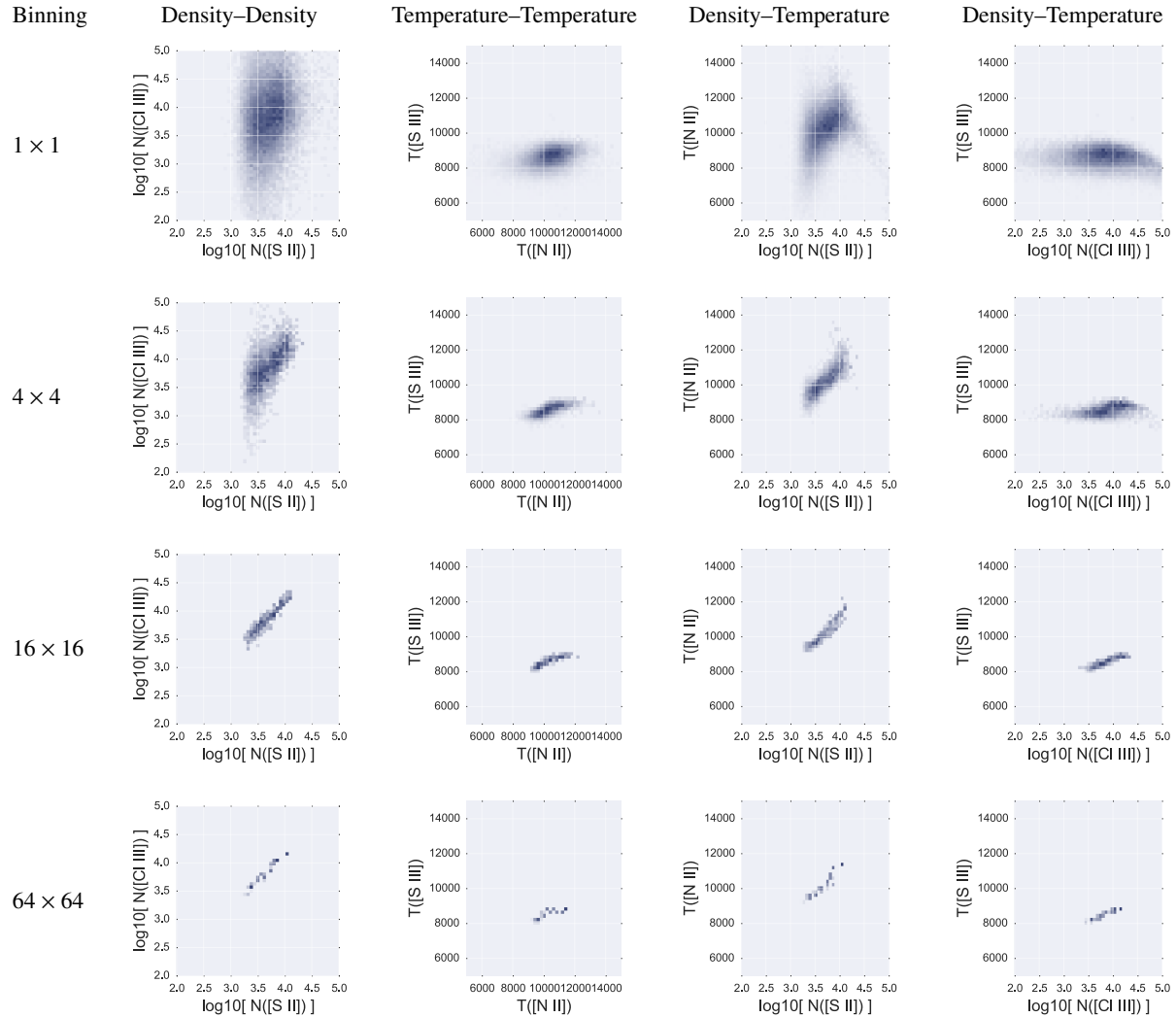


Fig. 9.— Correlations between derived densities and temperatures as a function of binning for the sweet spot.

2. Absorption lines

3. Fluorescent lines

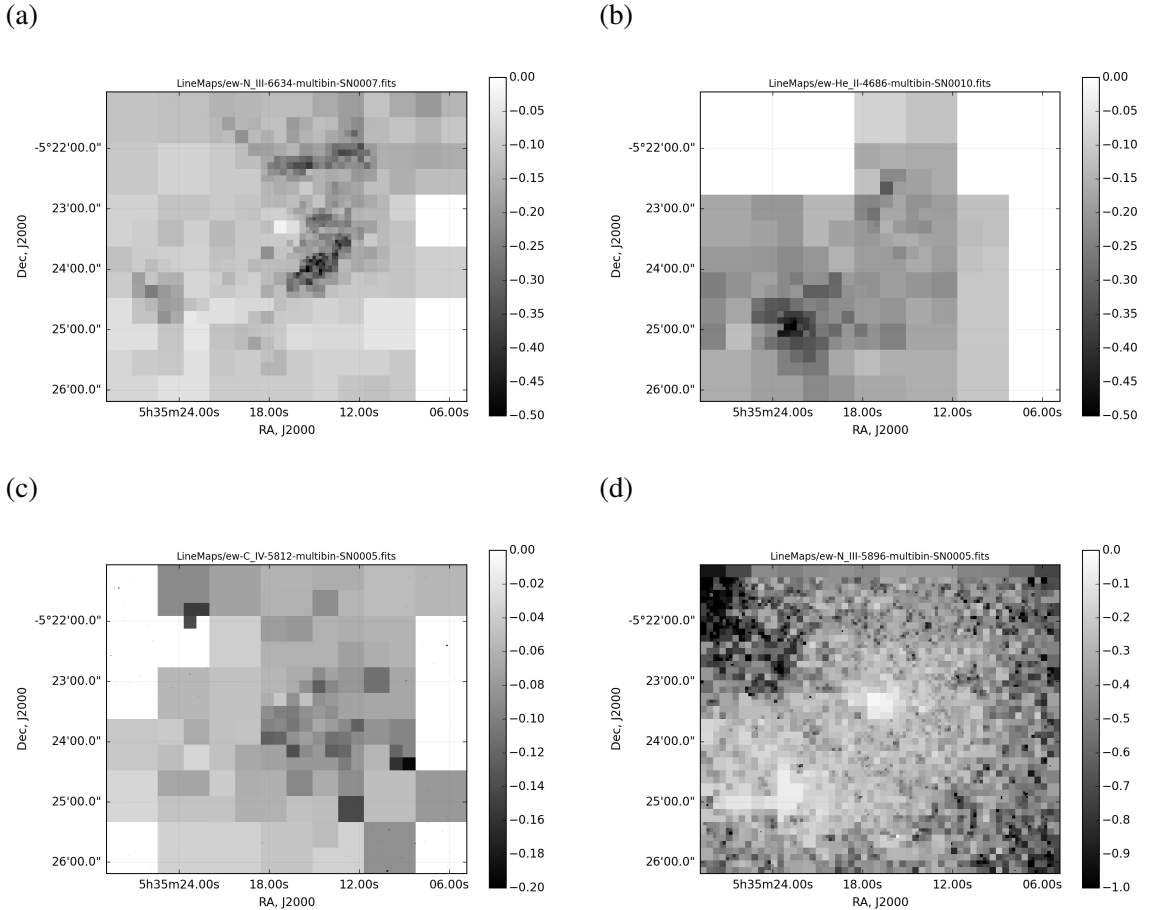


Fig. 10.— Equivalent width of selected absorption lines from the MUSE spectra, adaptively binned to give constant signal-to-noise ratios. (a) Mystery 6634 line. Traces absorption in PDR. (b) He II 4686 line. Scattered starlight from θ^2 Ori A (c) C IV 5812 line. Scattered starlight from Trapezium. (d) N III 5896 line. Scattered starlight, but filled in by fluorescent excitation in nebula?

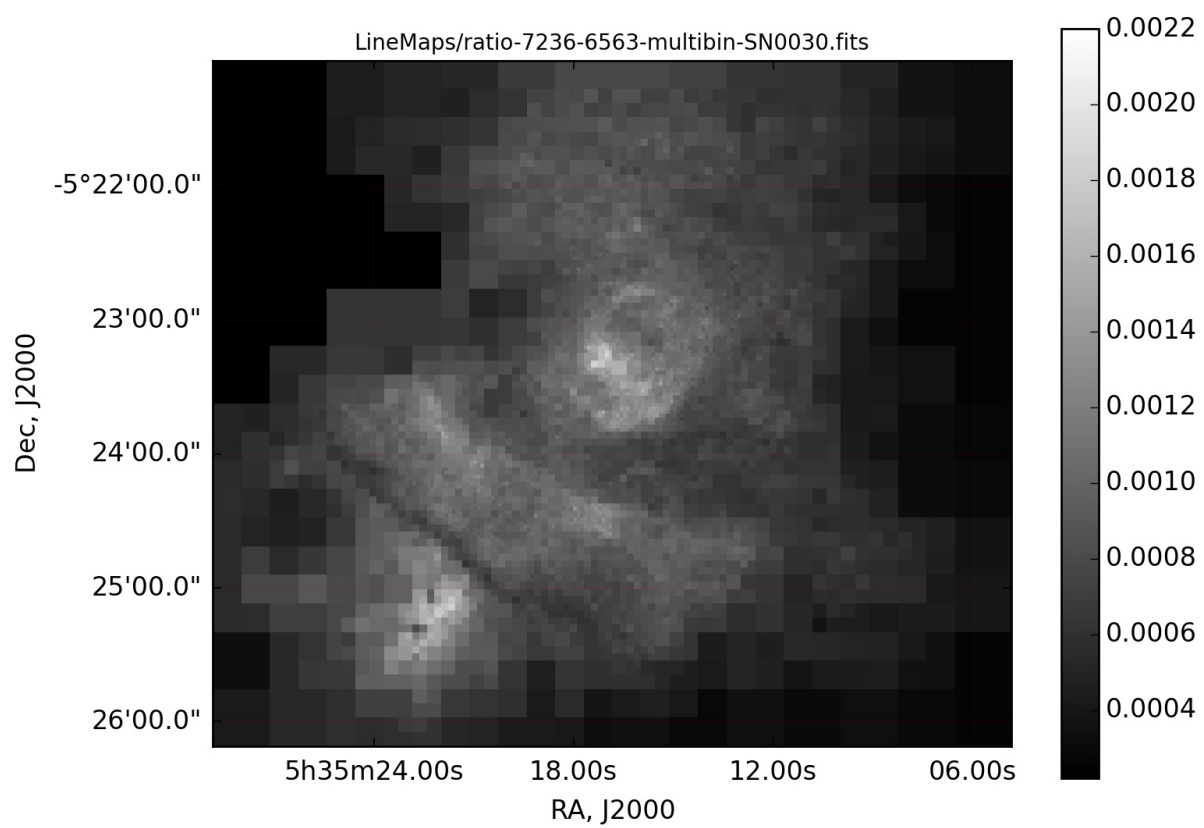


Fig. 11.— Ratio of C II 7236 to H α

A. New calibration of the WFC3 filters with MUSE

(Weilbacher et al. 2015)

B. Comparison of spectrally derived and filter-derived line ratios

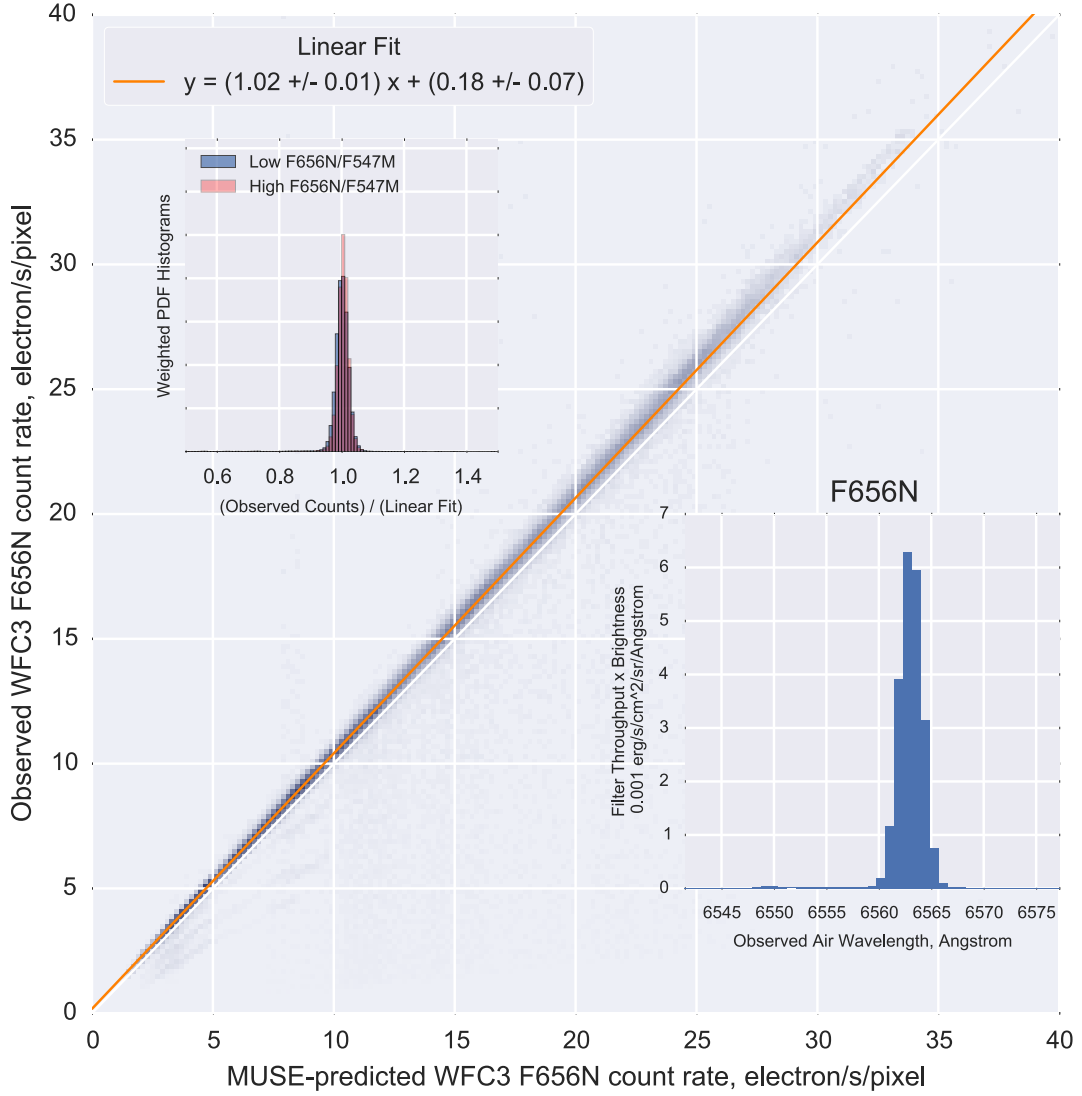


Fig. 12.— Results of spectrophotometric calibration of the WFC3 F656N filter. The vertical axis of the principal plot is the observed WFC3 filter count rate after resampling at the 0.2'' pixel size of the MUSE spectrophotometric observations. The horizontal axis of the principal plot is the predicted count rate calculated by folding the MUSE spectrum through the nominal WFC3 filter throughput profile. The grayscale intensity represents the two-dimensional histogram over the entire usable WFC3 field of these two quantities, weighted by the count rate of each pixel. The red line is the optimum linear fit to the relationship. The lower right inset plot shows the product of the MUSE spectrum (integrated over the entire field) and the filter throughput profile. The upper left inset plot shows the distribution of deviations from the linear fit for two subsamples of pixels: the red histogram shows the subsample with larger than average line/continuum ratio, while the blue histogram shows the subsample with smaller than average line/continuum ratio.

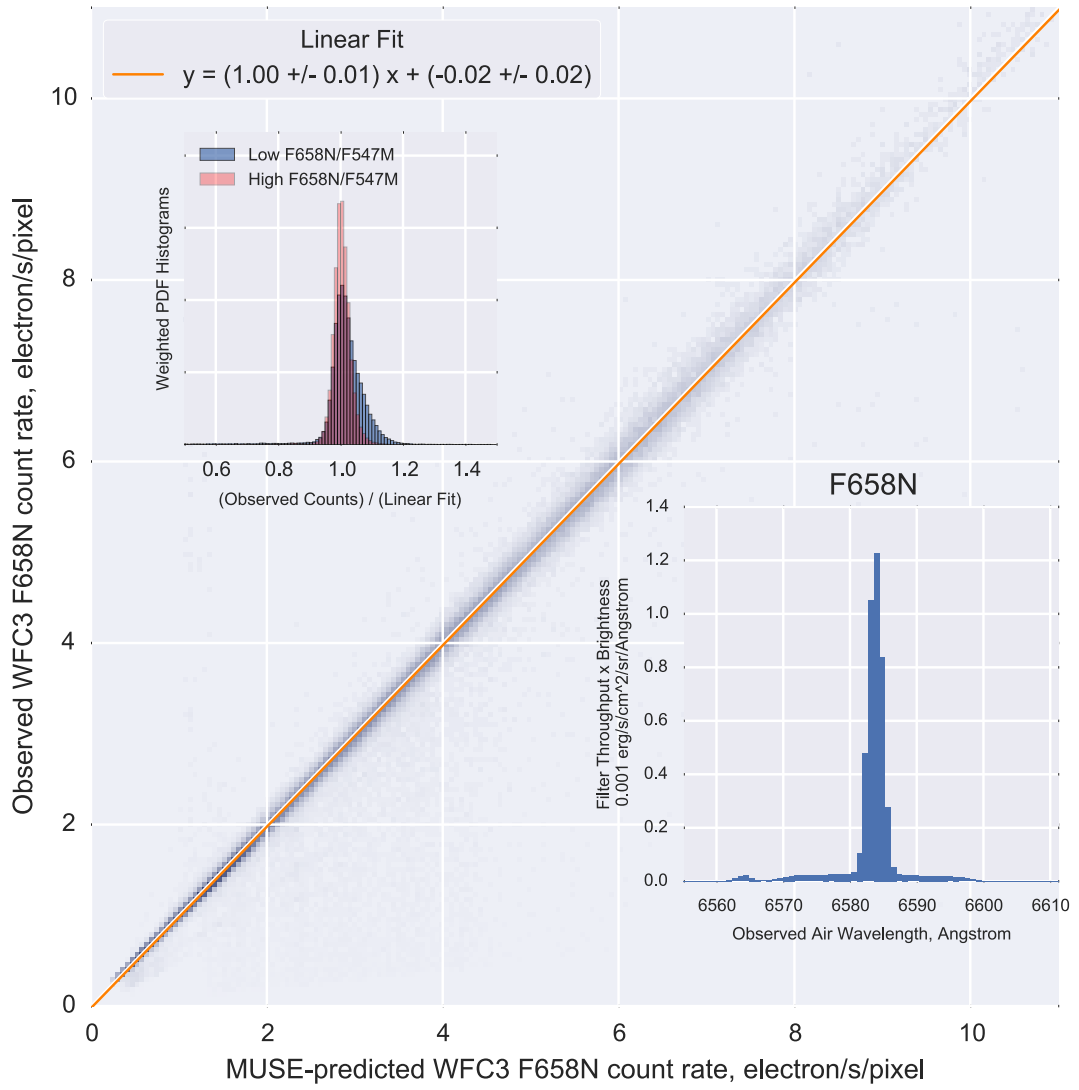


Fig. 13.— F658N

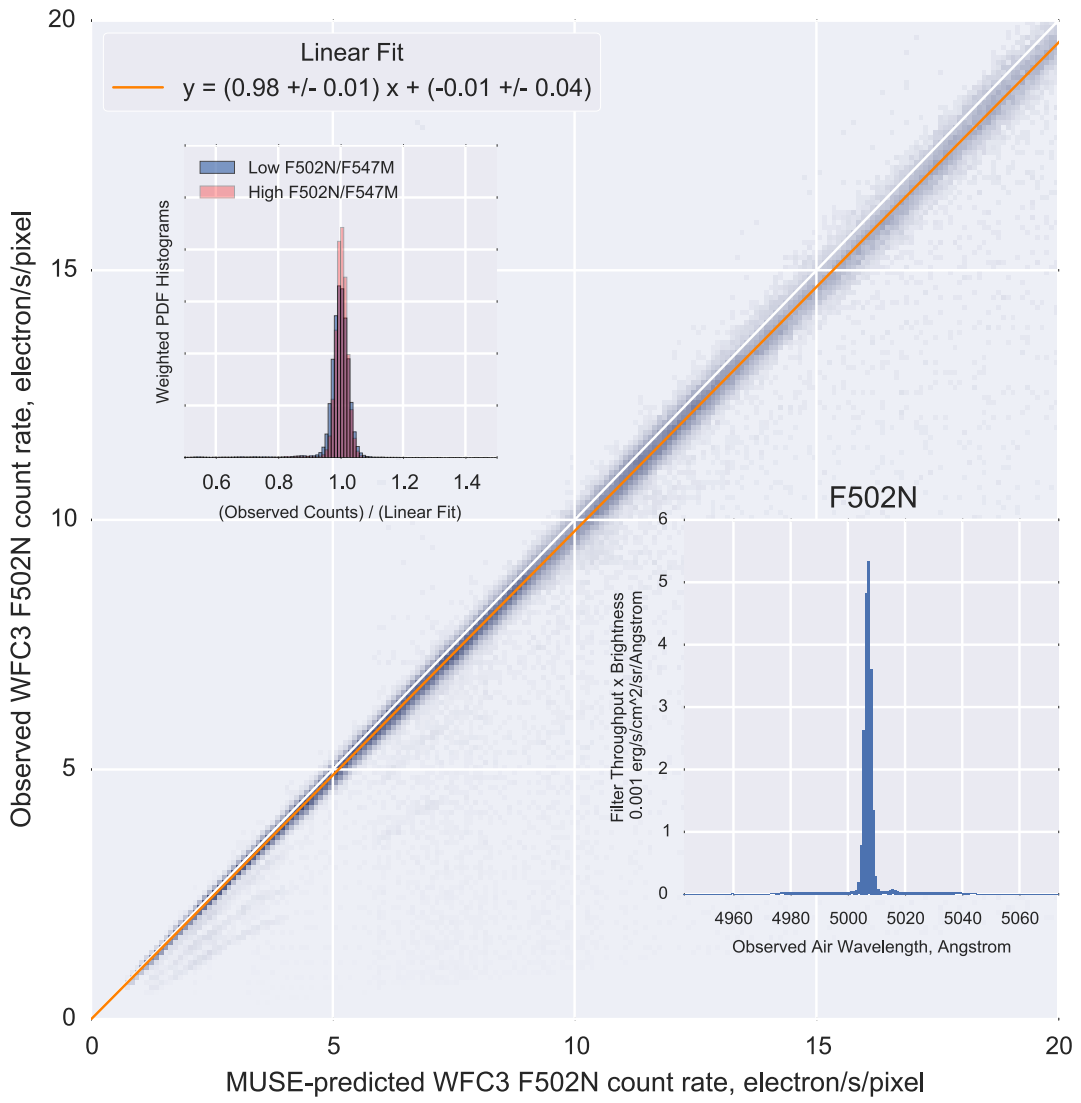


Fig. 14.— F502N

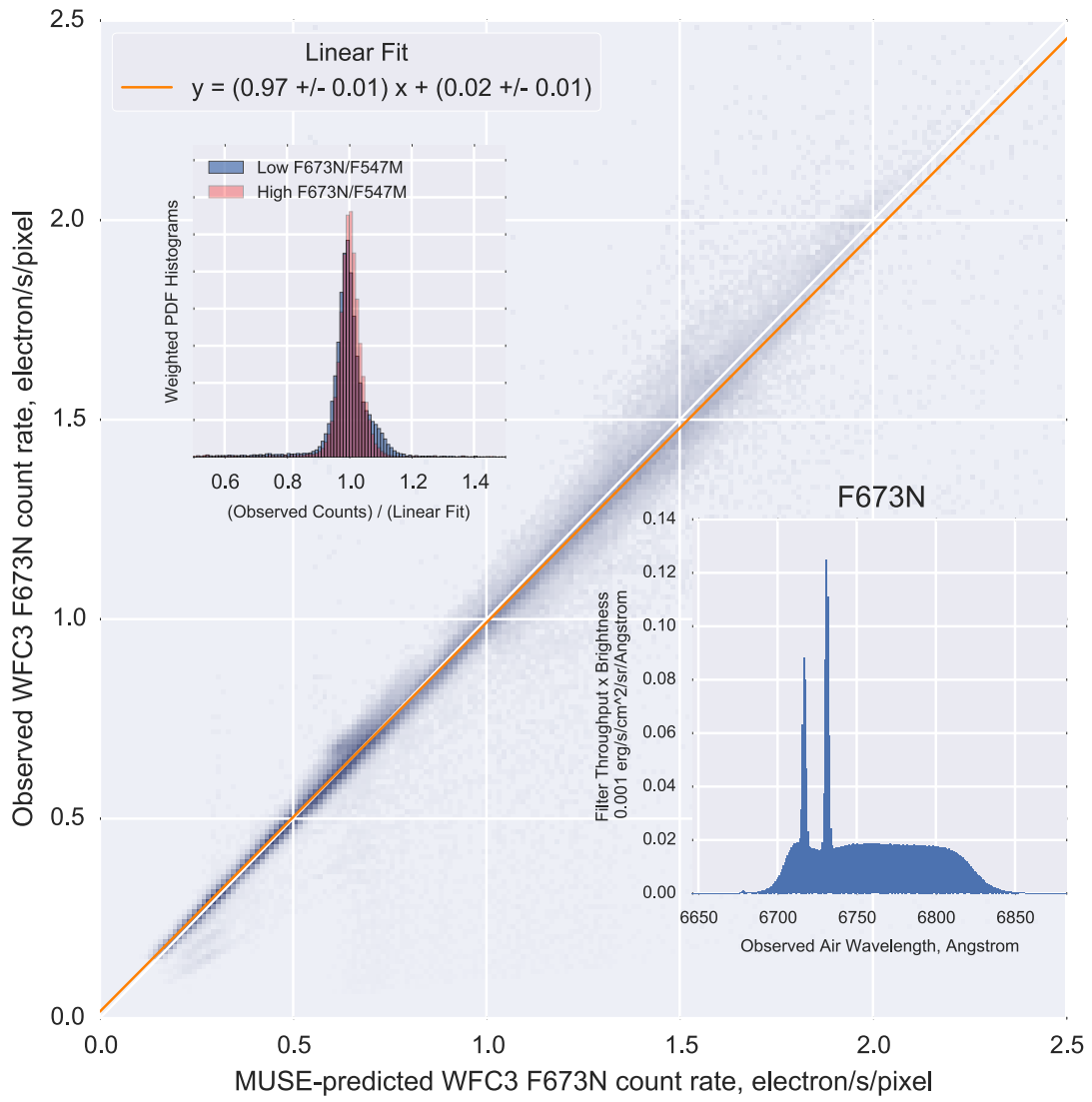


Fig. 15.— F673N

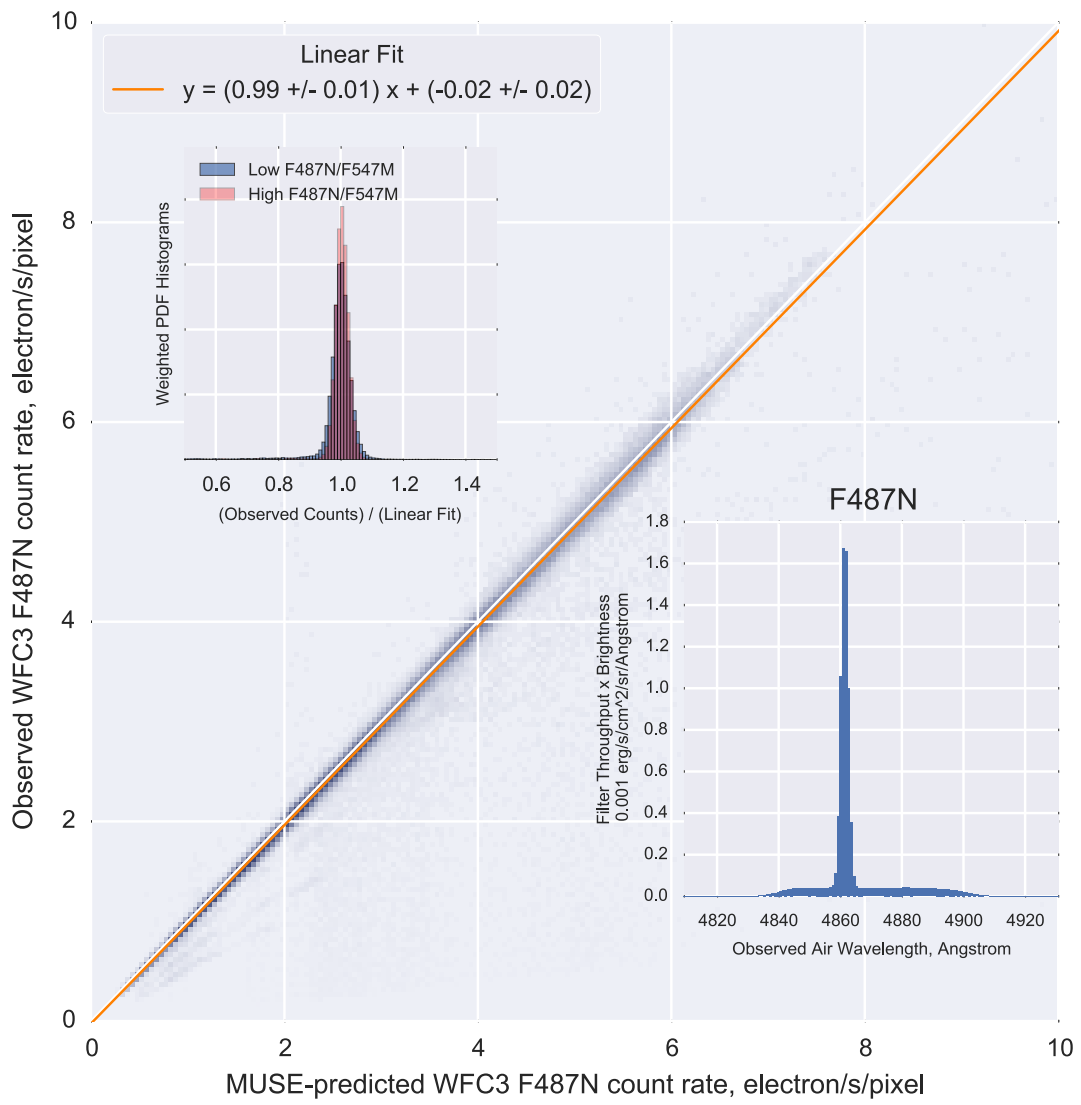


Fig. 16.— F487N

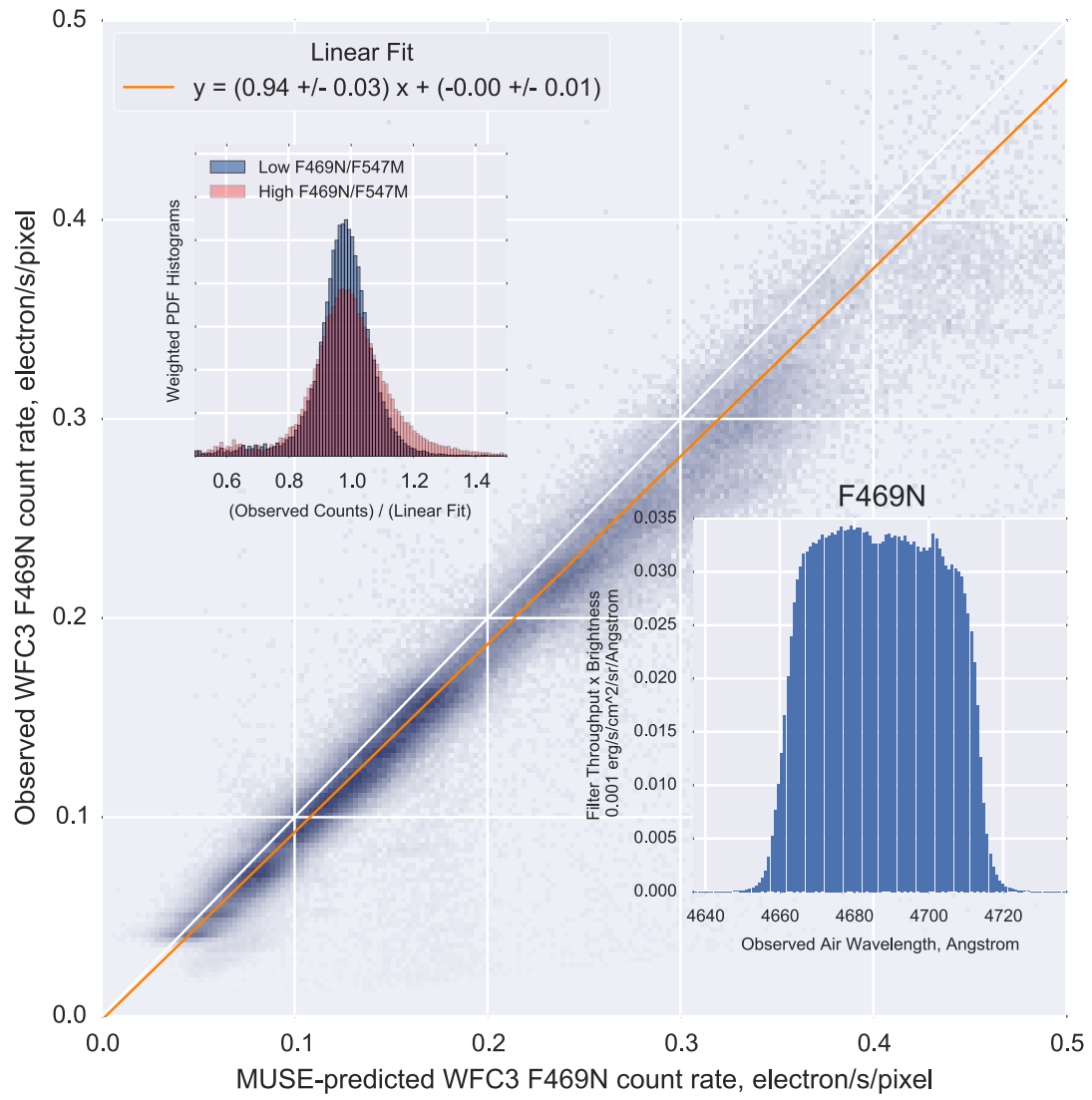


Fig. 17.— F469N

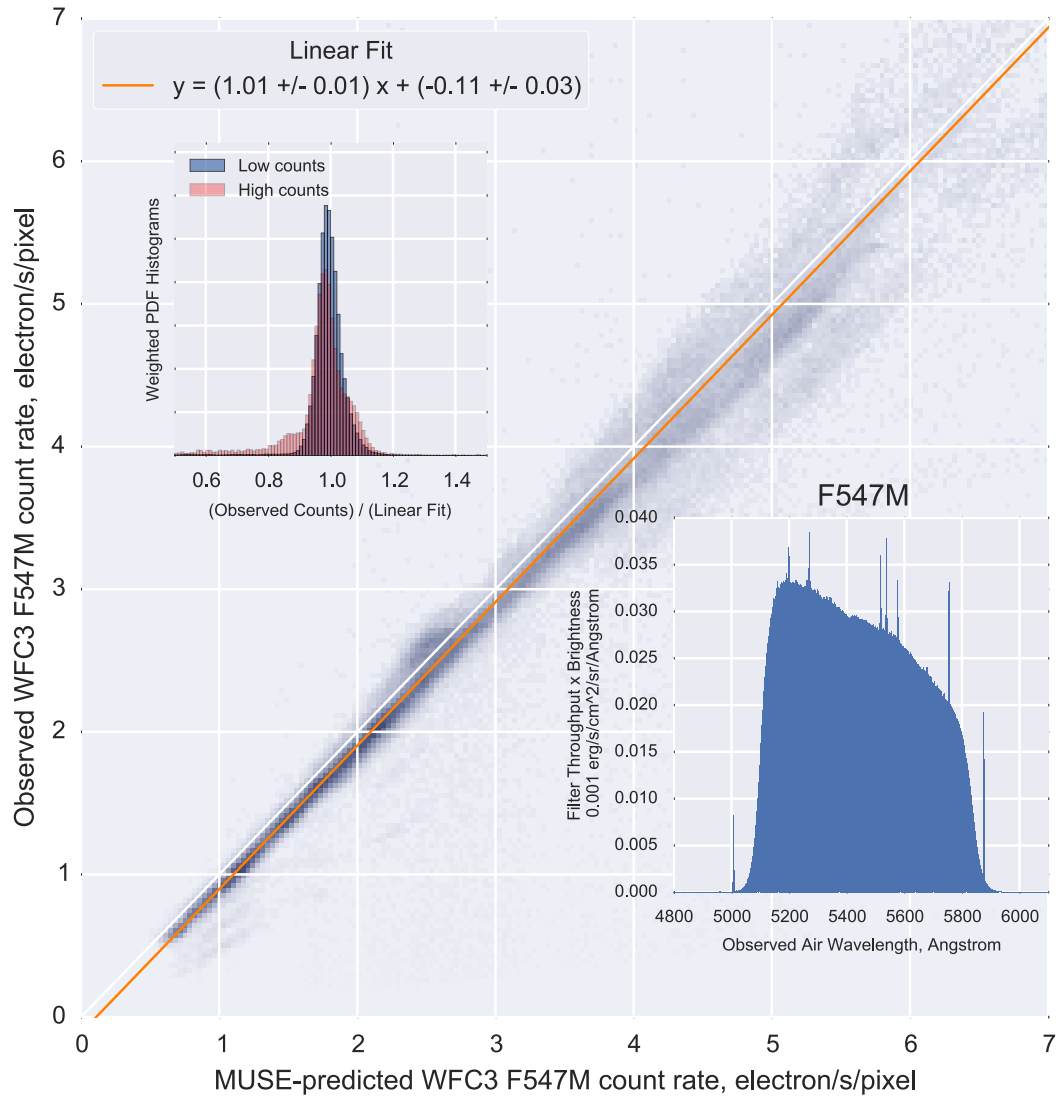


Fig. 18.— F547M

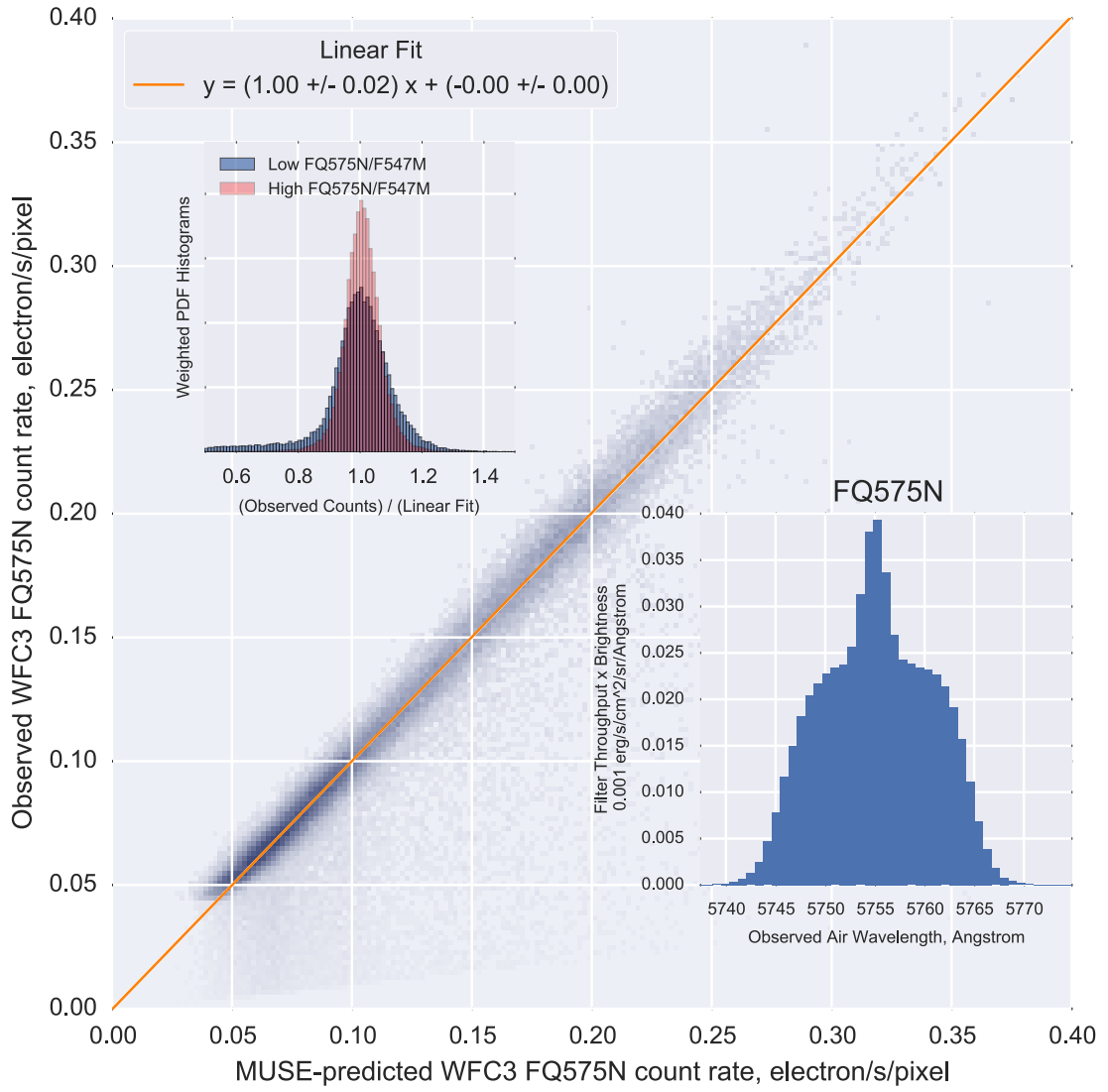


Fig. 19.— FQ575N

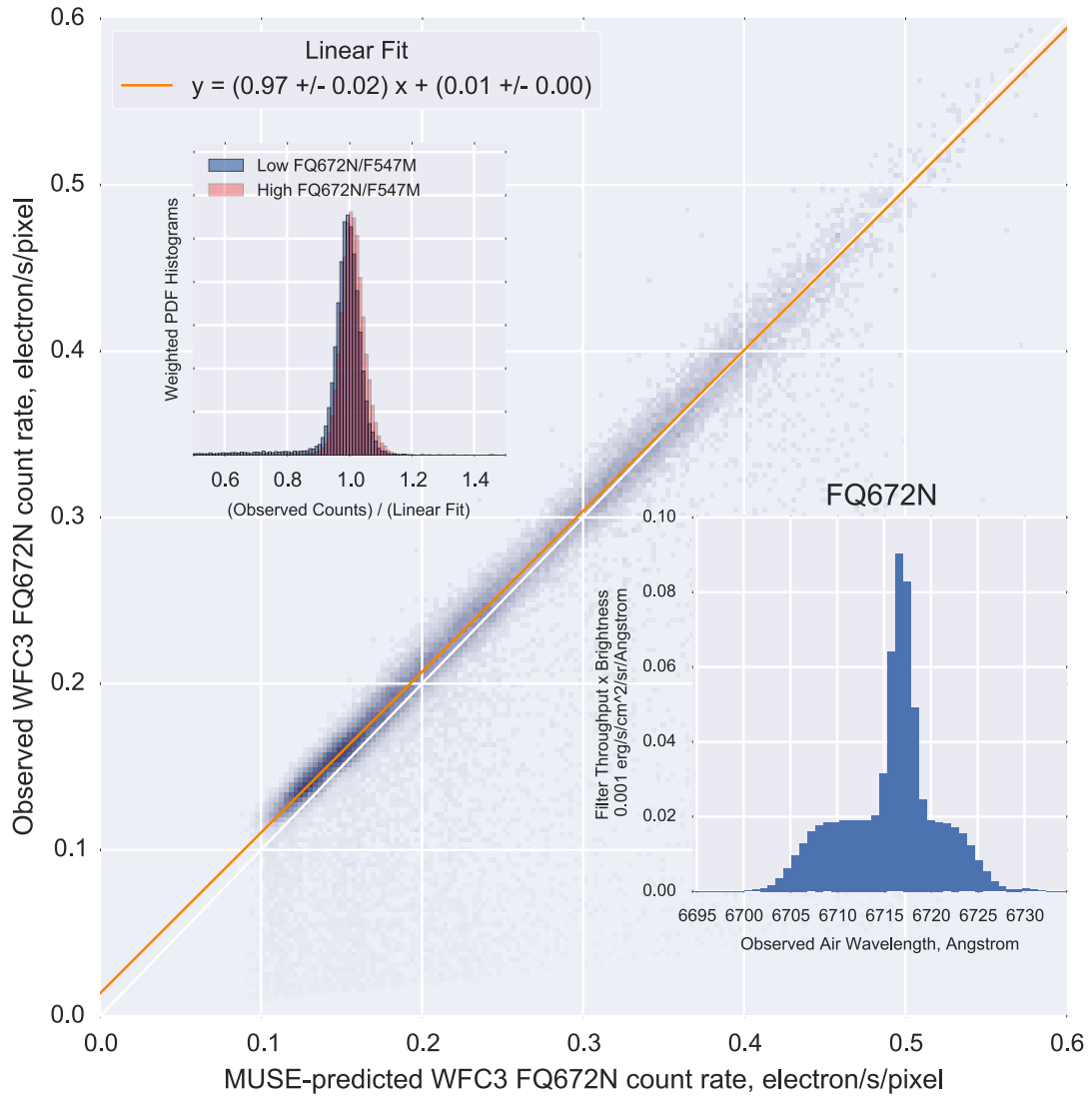


Fig. 20.— FQ672N

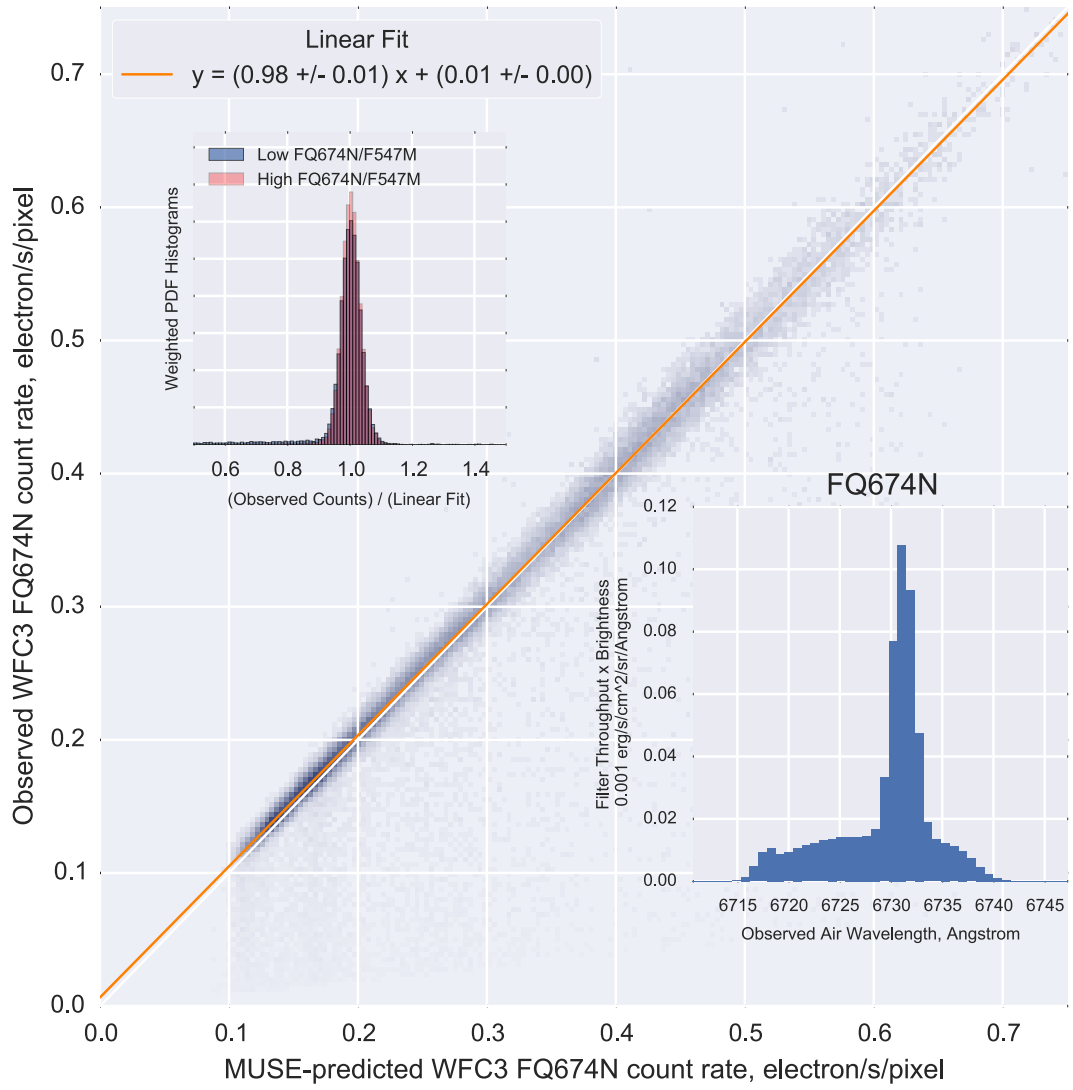


Fig. 21.— FQ674N

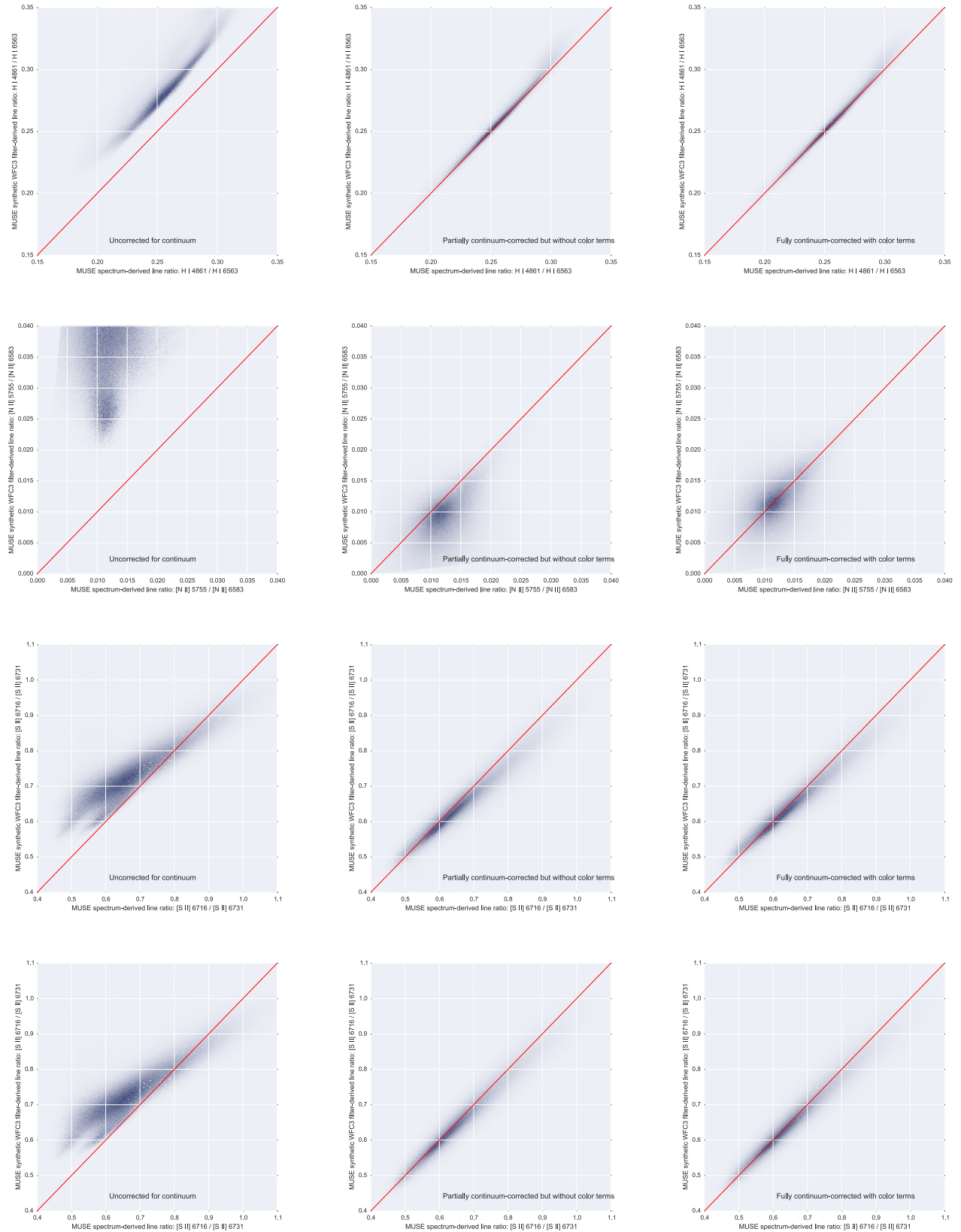


Fig. 22.— Successive improvements in line ratio estimation using synthetic filters with the MUSE dataset

REFERENCES

Weilbacher, P. M., et al. 2015, A&A, 582, A114